dicates that in this case the reaction goes by an outer-sphere mechanism. The largest deviation is in the case of uranium. This may be due to the uncertainty in the value of the redox potential or the value of k^{ht} used.

Reasons for the variation between observed and calculated rate parameters, in reactions characterized by such ΔG° values as exhibited by these compounds, have been discussed by Marcus and Sutin[14] and extensively documented by Weaver and Yee.[15] Additional insight into the mechanism of these reactions requires additional studies using actinides that will extend to ΔG° range.

Registry No. CO_3^-, 16518-46-0; $[UO_2(CO_3)_3]^{5-}$, 20274-15-1; $[UO_2(CO_3)_3]^{4-}$, 17872-00-3; $[NpO_2(CO_3)_3]^{5-}$, 64520-72-5; $[NpO_2(CO_3)_3]^{4-}$, 64519-49-9; $[PuO_2(CO_3)_3]^{5-}$, 89873-83-6; $[PuO_2(CO_3)_3]^{4-}$, 89850-08-8.

(14) Marcus, R. A.; Sutin, N. *Inorg. Chem.* **1975**, *14*, 213.

(15) Weaver, M. J.; Yee, E. L. *Inorg. Chem.* **1980**, *19*, 1936.
(16) Nash, K.; Mulac, W. A.; Noon, M.; Fried, S.; Sullivan, J. C. *J. Inorg. Nucl. Chem.* **1981**, *43*, 897.
(17) Pikaev, A. K.; Ershov, B. G.; Marakov, I. E. *J. Phys. Chem.* **1975**, *79*, 3027.

Contribution from the Department of Chemistry, University of Virginia, Charlottesville, Virginia 22901

Hypersensitivity in the 4f → 4f Absorption Spectra of Neodymium(III) Complexes in Aqueous Solution

EILEEN M. STEPHENS, KARL SCHOENE, and F. S. RICHARDSON*

Received July 25, 1983

Absorption difference spectra are reported for six different Nd^{3+}/ligand systems vs. $NdCl_3$ in aqueous solution. These spectra were obtained as a function of Nd^{3+}/ligand solution pH. The ligands differ with respect to their donor (ligating) atoms, their substituent groups, their chelation geometries, and their total coordination numbers. However, each includes two carboxylate groups in its structure. The difference spectra (ΔA vs. λ) and oscillator strength ratios [f(complex):f($NdCl_3$(aq))] associated with the $^4I_{9/2} \rightarrow {}^4G_{5/2}$, $^2G_{7/2}$ absorption band (570–595 nm) exhibit *hypersensitive* behavior with respect to ligand type and solution pH. The variations observed in the ΔA spectra and in the oscillator strength ratios, with respect to both ligand type and solution pH, are rationalized in terms of ligand structure, ligand coordination properties, and ligand field geometry. Intensity calculations, based on a theoretical model for 4f → 4f electric dipole strengths, are carried out for a set of model structures assumed to be similar to those of several of the complexes studied experimentally. The results of these calculations are compared to the observed intensity data and are discussed in terms of spectra–structure correlations in the $^4I_{9/2} \rightarrow {}^4G_{5/2}$, $^2G_{7/2}$ "hypersensitive" transition region.

Introduction

Among the trivalent lanthanide ions, neodymium(III) has perhaps been used most frequently as an absorption probe of lanthanide–ligand interactions in solution media. The absorption band associated with the nearly degenerate $^4I_{9/2} \rightarrow {}^4G_{5/2}$ and $^2G_{7/2}$ transitions of Nd(III) exhibits strong "hypersensitive" behavior,[1-5] making it especially suitable for probing the coordination environment about the Nd(III) ion. The total (integrated) intensity, intensity distribution, and energy barycenter of this band are each strongly modulated by ligand coordination properties. Furthermore, this band occurs in a readily accessible region of the spectrum (~ 570–590 nm), and it is not overlapped by any other Nd(III) absorptions.

As a class, nearly all the hypersensitive multiplet–multiplet (4f → 4f) transitions of lanthanide ions share a common set of selection rules at the intermediate-coupling level. These rules are just those of radiative electric quadrupolar processes for 4f → 4f transitions.[1,2,6-9] However, it is nearly certain that essentially all of the observed intensity in these transitions is electric dipolar in nature. A number of proposals have been offered regarding the intensity mechanisms operative in these transitions,[1,2] and it is likely that each of the proposed mechanisms contributes to the observed intensities (and their *hypersensitivity* to the ligand environment). The most commonly invoked mechanism for hypersensitivity is that contained in the "inhomogeneous dielectric" theory of Jørgensen and Judd[6] and in the "ligand polarization" model proposed by Mason, Peacock, and Stewart.[1,7] According to this mechanism, the electric dipolar components of the radiation field induce a set of transient (electric) dipoles in the ligand environment that may couple to the 4f-electron distributions via electrostatic quadrupole (Ln)–dipole (ligand) interactions. These quadrupole-induced dipole interactions can lead to large amplifications of the 4f → 4f electric quadrupole transition probabilities. Thus, the observed spectral transition is electric quadrupolar with respect to the 4f → 4f processes involved but is electric dipolar with respect to the overall radiation–molecule interaction processes. This accounts for the hypersensitive transitions often being referred to as "pseudoquadrupolar" in nature. It also accounts for the correlation of hypersensitivity behavior with ligand (electric) dipolar polarizability.

(1) Peacock, R. D. *Struct. Bonding (Berlin)* **1975**, *22*, 83.
(2) Henrie, D. E.; Fellows, R. L.; Choppin, G. R. *Coord. Chem. Rev.* **1976**, *18*, 199.
(3) Choppin, G. R.; Henrie, D. E.; Buijs, K. *Inorg. Chem.* **1966**, *5*, 1743.
(4) Henrie, D. E.; Choppin, G. R. *J. Chem. Phys.* **1968**, *49*, 477.
(5) Bukietynska, K.; Choppin, G. R. *J. Chem. Phys.* **1970**, *52*, 2875.
(6) Jørgensen, C. K.; Judd, B. R. *Mol. Phys.* **1964**, *8*, 281.
(7) Mason, S. F.; Peacock, R. D.; Stewart, B. *Mol. Phys.* **1975**, *30*, 1829.
(8) Richardson, F. S.; Saxe, J. D.; Davis, S. A.; Faulkner, T. R. *Mol. Phys.* **1981**, *42*, 1401.
(9) Judd, B. R. *J. Chem. Phys.* **1979**, *70*, 4830.

0020-1669/84/1323-1641$01.50/0

In the present paper we report absorption results obtained on a series of neodymium(III) complexes in aqueous solution under variable pH conditions. Each of the ligands included in this study contains two terminal carboxylate groups (ensuring relatively strong Ln–ligand binding even at low pH), but these ligands differ from one another with respect to the remainder of their donor groups and their nonligating substituent groups. The main objectives of the study were to determine if, and by how much, the 4f → 4f absorption spectra reflect differences in ligand coordination properties and structure and to correlate any observed spectral differences with specific structural parameters. In each case, spectra were measured throughout the 340–780-nm region, but special attention was given to the hypersensitive $^4I_{9/2} \rightarrow {}^4G_{5/2}, {}^2G_{7/2}$ transition region (~570–590nm).

Intensity calculations, based on a previously described intensity model,[8] are also reported for several "idealized" structures chosen to represent the main coordination properties of several of our real systems (in aqueous solution a pH >7).

The ligands included in this study were oxydiacetate (ODA), dipicolinate (DPA), iminodiacetate (IDA), (methylimino)diacetate (MIDA), *N,N'*-ethylenebis(2-(*o*-hydroxyphenyl))glycinate (EHPG),[10] and malate (MAL). Both ODA and DPA are terdentate ligands that form pairs of coplanar (5-membered) chelate rings with a lanthanide ion.[11,12] The only difference between these two ligands is in the nature of their respective central donor moieties—an ether oxygen in ODA and a pyridyl group in DPA. The IDA and MIDA ligands are also potentially terdentate, but in these systems coplanarity of the chelate rings is precluded by the preferred sp^3 hybridization on the central nitrogen donor atoms.[13] The only difference between IDA and MIDA is the H vs. CH_3 substituent on the nitrogen donor atom. The EHPG ligand is potentially hexadentate with two carboxylate donor moieties, two amino donor groups, and two phenolate donor moieties. However, for 1:1 Ln^{3+}:EHPG in aqueous solution, hexadentate chelation is not complete until pH >8.[14] The malate ligand can coordinate in a bidentate fashion via its two carboxylate moieties, and there is evidence that its hydroxyl group also enters the first coordination sphere about a lanthanide ion.[15] We have, then, a set of ligands that differ with respect to their donor atoms, chelation modes, conformational properties, and substituent groups. It is expected that each of these structural differences will be reflected in the intensity behavior of the Nd(III) $^4I_{9/2} \rightarrow {}^4G_{5/2}, {}^2G_{7/2}$ hypersensitive transitions.

Experimental Section

$NdCl_3 \cdot 6H_2O$ (99.99%) was purchased from Aldrich and was used without futher purification. Oxydiacetic acid ($ODAH_2$) and (methylimino)diacetic acid ($MIDAH_2$) were also purchased from Aldrich and used without further purification. Iminodiacetic acid ($IDAH_2$) and disodium dipicolinate ($DPANa_2$) were purchased from Sigma. *N,N'*-ethylenebis(2-(*o*-hydroxyphenyl))glycine (EHPG) was purchased from Pfaltz and Bauer and was purified and handled according to the procedures described in ref 14. D,L-Malic acid was purchased from Aldrich.

All spectroscopic measurements reported here were carried out on aqueous solution samples in which $[Nd^{3+}]$ = 10mM. For the EHPG studies, $[Nd^{3+}]$:[EHPG] = 1:1, whereas for all of the other ligand studies, $[Nd^{3+}]$:[ligand] = 1:3. Solution pH adjustments were made by using dilute NaOH. Absorption spectra were recorded on a Cary 17 D spectrophotometer with the samples contained in 1-cm quartz cells. All absorption *difference* spectra were recorded with $NdCl_3$(aq) in the reference beam and the $NdCl_3$/ligand/water system in the sample beam.

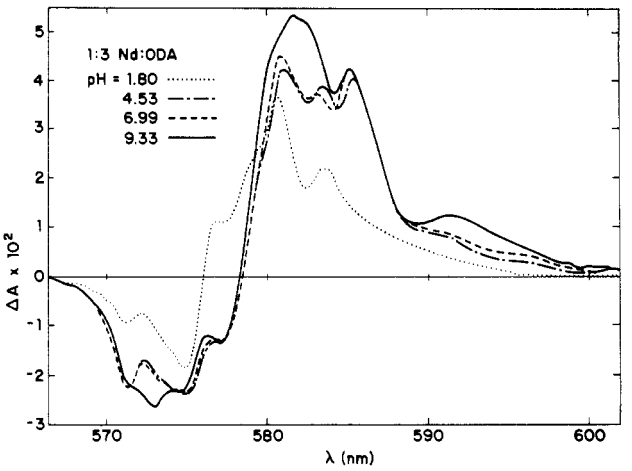

Figure 1. Absorption difference spectra recorded in the $^4I_{9/2} \rightarrow {}^4G_{5/2}, {}^2G_{7/2}$ transition region for 1:3 Nd^{3+}:ODA in aqueous solution.

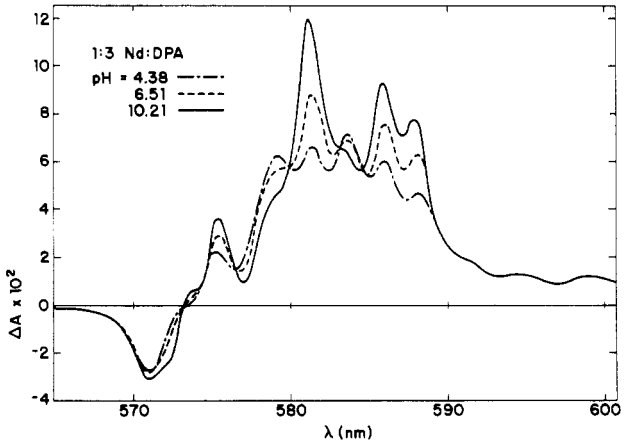

Figure 2. Absorption difference spectra recorded in the $^4I_{9/2} \rightarrow {}^4G_{5/2}, {}^2G_{7/2}$ transition region for 1:3 Nd^{3+}:DPA in aqueous solution.

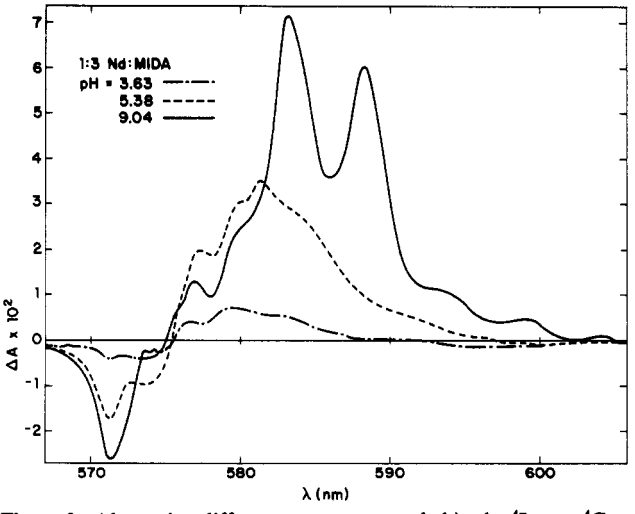

Figure 3. Absorption difference spectra recorded in the $^4I_{9/2} \rightarrow {}^4G_{5/2}, {}^2G_{7/2}$ transition region for 1:3 Nd^{3+}:MIDA in aqueous solution.

Oscillator strengths, defined here by

$$f = 4.32 \times 10^{-9} \int \epsilon(\bar{\nu})\, d\bar{\nu} \quad (1)$$

were obtained by evaluating $\int \epsilon(\bar{\nu})\, d\bar{\nu}$ over the transition region of interest. *Differential* oscillator strengths

$$\Delta f = f(\text{complex}) - f(NdCl_3(aq)) = 4.32 \times 10^{-9} \int \Delta\epsilon(\bar{\nu})\, d\bar{\nu} \quad (2)$$

were determined directly from the $\Delta\epsilon(\bar{\nu})$ vs. $\bar{\nu}$ difference spectra.

(10) The alternative, and more proper, name for EHPG is *N,N'*-bis(2-hydroxyphenyl)ethylenedinitrilo-*N,N'*-diacetate.
(11) Albertsson, J. *Acta Chem. Scand.* **1968**, *22*, 1563; *Ibid.* **1970**, *24*, 3527.
(12) Albertsson, J. *Acta Chem. Scand.* **1970**, *24*, 1213; *Ibid.* **1972**, *26*, 985, 1005, 1023.
(13) Oskarsson, A. *Acta Chem. Scand.* **1971**, *25*, 1206.
(14) Salama, S.; Richardson, F. S. *Inorg. Chem.* **1980**, *19*, 635.
(15) Salama, S.; Richardson, F. S. *Inorg. Chem.* **1980**, *19*, 629.

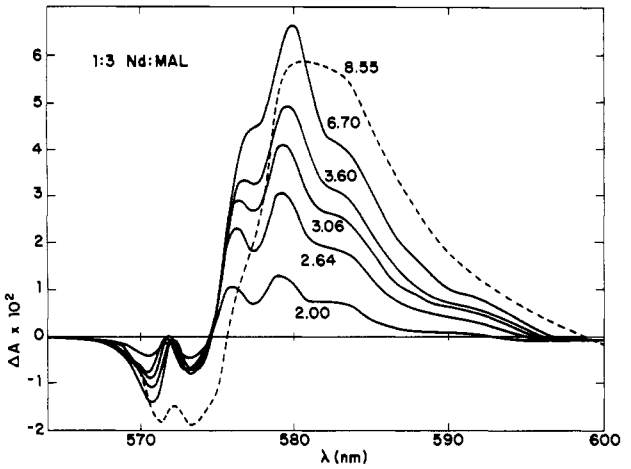

Figure 4. Absorption difference spectra recorded in the $^4I_{9/2} \rightarrow {}^4G_{5/2}$, $^2G_{7/2}$ transition region for 1:3 Nd^{3+}:MAL in aqueous solution.

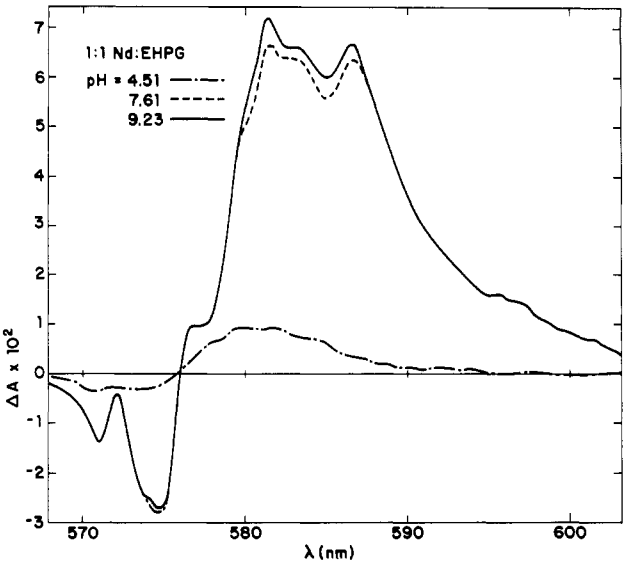

Figure 5. Absorption difference spectra recorded in the $^4I_{9/2} \rightarrow {}^4G_{5/2}$, $^2G_{7/2}$ transition region for 1:1 Nd^{3+}:EHPG in aqueous solution.

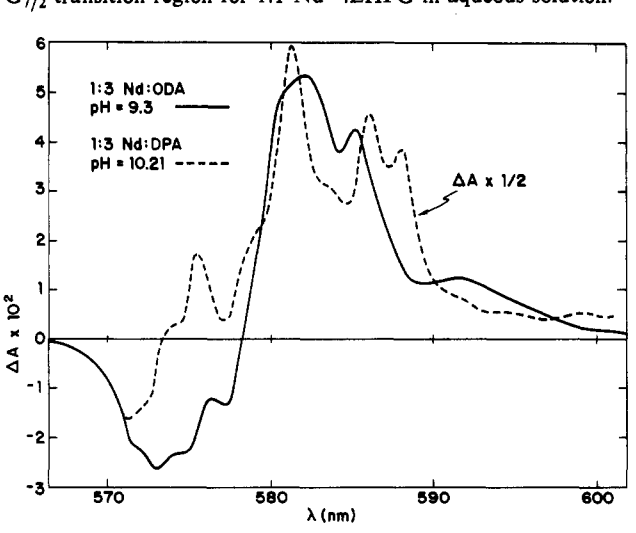

Figure 6. Comparison of absorption difference spectra obtained for 1:3 Nd^{3+}:ODA and 1:3 Nd^{3+}:DPA in aqueous solution at high pH.

Results

Absorption difference spectra obtained in the $^4I_{9/2} \rightarrow {}^4G_{5/2}$, $^2G_{7/2}$ transition region are shown in Figures 1–9. In each case, $\Delta A < 0$ on the higher energy side of this transition region and $\Delta A > 0$ on the lower energy side. This indicates a *red shift* in the transition barycenter upon complexation of the Nd(III)

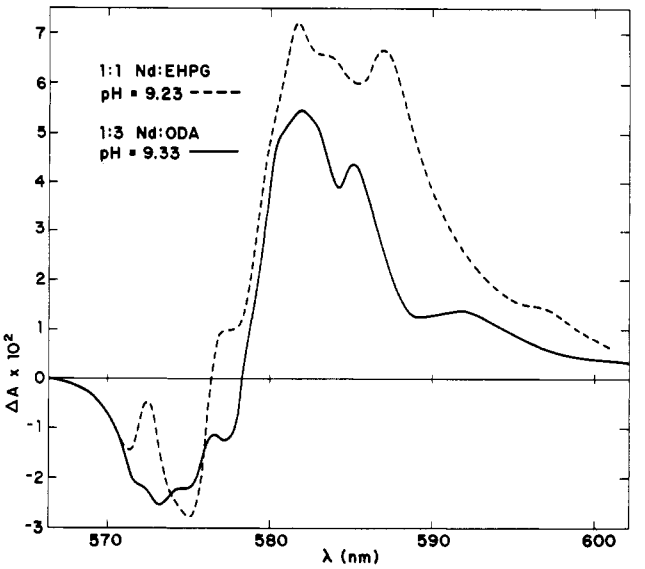

Figure 7. Comparison of absorption difference spectra obtained for 1:1 Nd^{3+}:EHPG and 1:3 Nd^{3+}:ODA in aqueous solution at high pH.

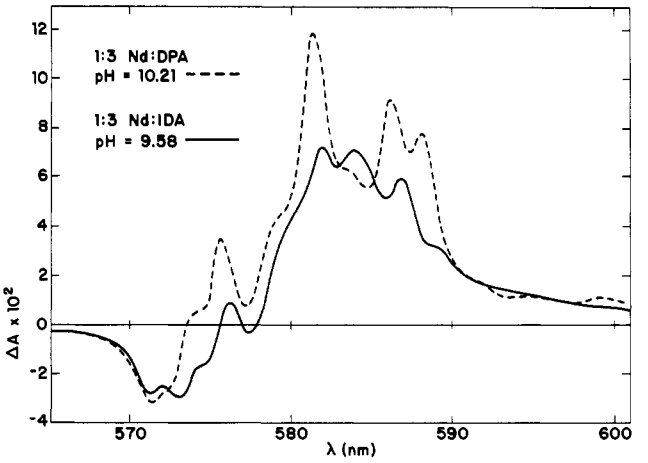

Figure 8. Comparison of absorption difference spectra obtained for 1:3 Nd^{3+}:DPA and 1:3 Nd^{3+}:IDA in aqueous solution at high pH.

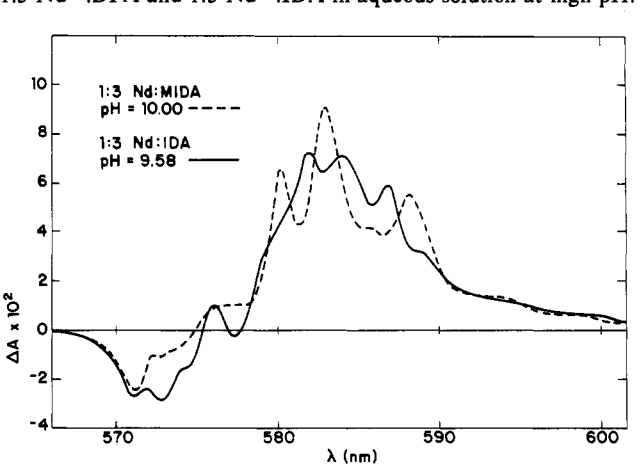

Figure 9. Comparison of absorption difference spectra obtained for 1:3 Nd^{3+}:MIDA and 1:3 Nd^{3+}:IDA in aqueous solution at high pH.

by the organic ligands. Furthermore, in each case the observed $|\Delta A|$ increases with increasing solution pH, indicating that the $^4I_{9/2} \rightarrow {}^4G_{5/2}$, $^2G_{7/2}$ oscillator strengths increase with increasing complexation of the Nd(III) by the organic ligands. The latter is a manifestation of the *hypersensitivity* associated with the $^4I_{9/2} \rightarrow {}^4G_{5/2}$, $^2G_{7/2}$ absorption. Experimentally determined values of Δf and f(complex):$f(NdCl_3(aq))$ are listed in Table I for selected pH values for each system examined in this study.

Table I. Experimentally Determined Oscillator Strengths in the $^4I_{9/2} \rightarrow {}^4G_{5/2}, {}^2G_{7/2}$ Transition Region

system	pH	$\Delta f^a/10^{-6}$	f(complex): $f(NdCl_3(aq))^b$
1:3 Nd:ODA	9.33	4.24	1.49
	1.86	3.46	1.40
1:3 Nd:DPA	10.21	10.57	2.22
	4.38	8.88	2.03
1:3 Nd:IDA	9.58	9.35	2.08
	2.41	0.98	1.11
1:3 Nd:MIDA	10.00	8.86	2.02
	2.71	0.92	1.11
1:3 Nd:MAL	9.78	7.48	1.86
	2.00	1.66	1.19
1:1 Nd:EHPG	9.23	10.96	2.28
	4.51	1.47	1.17

[a] $\Delta f = f(\text{complex}) - f(NdCl_3(aq))$. See eq 2 of text. [b] $f(NdCl_3(aq)) = 8.65 \times 10^{-6}$.

Absorption difference spectra were in all cases recorded throughout the 340–780-nm region. However, without exception the $|\Delta A|$ values observed in the $^4I_{9/2} \rightarrow {}^4G_{5/2}, {}^2G_{7/2}$ transition region (~570–590 nm) were by far the largest.

Calculations

Energy level and intensity calculations were carried out for five different structures. Structure **1** has the formula NdL_9 and corresponds to a 9-coordinate $Nd^{3+}(aq)$ complex with D_{3h} point-group symmetry. NdL_9 (**1**) has a tricapped-trigonal-prism structure, and L is intended to represent a water molecule in a "united-atom" approximation. Neither the coordination number nor the geometry of $Nd^{3+}(aq)$ complexes is known; however, our structure **1** represents the most likely idealized structure for these species.[16]

Our structures **2** and **3** are the tris terdentate $Nd(ODA)_3^{3-}$ and $Nd(DPA)_3^{3-}$ complexes. The coordination polyhedron in each of these structures forms a *distorted*-tricapped-trigonal prism with trigonal-dihedral (D_3) symmetry. Carboxylate donor atoms form the top and bottom triangles of the prism and the equatorial sites are occupied by the middle donor atoms of the respective ligands. In each case, the terdentate ligands stretch diagonally across the rectangular faces of the trigonal prism in the so-called meridional (or *mer*) isomeric form (see Figure 15 of Favas and Kepert[17]). Our structures **2** and **3** correspond to those found for various $Ln(ODA)_3^{3-}$ and $Ln(DPA)_3^{3-}$ complexes in the solid state. They also represent the most likely structures of the *majority* species in neutral-to-basic aqueous solutions of 1:3 Nd^{3+}:ODA and Nd^{3+}:DPA.[18]

Our structures **4** and **5** are the tris terdentate $Nd(IDA)_3^{3-}$ and $Nd(MIDA)_3^{3-}$ complexes, respectively. The coordination polyhedra in these structures are also of the tricapped-trigonal-prism form, but in these systems the ligands wrap around the prism in a facial (or *fac*) isomeric configuration (see Figure 15 of Favas and Kepert[17]). The overall symmetry of structures **4** and **5** is C_{3h}. It has been proposed that in neutral-to-basic aqueous solutions of 1:3 Ln^{3+}:IDA and Ln^{3+}:MIDA the *majority* of species have structures similar to **4** and **5**.[18,19]

Our structures **2**–**5** have the following in common: (1) 9-fold coordination; (2) tricapped-trigonal-prism structures for the coordination polyhedra; (3) carboxylate donor atoms defining the top and bottom triangles of the trigonal prisms; (4) "nearly" D_{3h} symmetry for the coordination polyhedra. Their differences are in (1) how the chelate rings are arranged about the lanthanide ion (**2** and **3** differ from **4** and **5** in this respect), (2) chelate-ring conformations, and (3) the substituent groups attached to the middle donor atoms of the ligands. It is these differences that one may expect to be reflected in the absorption intensities of the hypersensitive transitions.

Table II. Neodymium(III) Electronic Parameters Used for Energy Level and Intensity Calculations[a]

$F_2/cm^{-1} = 321$	$\Xi(1,2)/cm^2\ erg^{-1} = -1.58 \times 10^{-6}$
$F_4/cm^{-1} = 46.3$	$\Xi(3,2)/cm^4\ erg^{-1} = 1.35 \times 10^{-22}$
$F_6/cm^{-1} = 4.69$	$\Xi(3,4)/cm^4\ erg^{-1} = 1.50 \times 10^{-22}$
$\alpha/cm^{-1} = 0.5611$	$\Xi(5,4)/cm^6\ erg^{-1} = -1.98 \times 10^{-38}$
$\beta/cm^{-1} = -117.2$	$\Xi(5,6)/cm^6\ erg^{-1} = -1.62 \times 10^{-38}$
$\gamma/cm^{-1} = 1321$	$\Xi(7,6)/cm^8\ erg^{-1} = 3.96 \times 10^{-54}$
$\zeta_{so}/cm^{-1} = 885$	$\langle r^2 \rangle/Å^2 = 0.2803$
	$\langle r^4 \rangle/Å^4 = 0.1883$
	$\langle r^6 \rangle/Å^6 = 0.2722$

[a] F_k denotes a Slater–Condon electrostatic radial parameter. α, β, and γ are configuration-interaction parameters,[20] and ζ_{so} denotes the radial spin-orbit coupling parameter. The $\Xi(t,\lambda)$ are *inter*configurational interaction parameters, as defined by Krupke,[21] and $\langle r^\lambda \rangle$ denotes a 4f-electron radial expectation value.[22]

Energy Level Calculations. Crystal field wave functions and energy levels for the $4f^3$ electronic configuration of Nd^{3+} are needed for carrying out electric dipole intensity calculations. These were obtained following the procedures reported in ref 8. The intermediate-coupling wave functions and multiplet barycenter energies were calculated by using a seven-parameter "free-ion" Hamiltonian and a SLJ basis set comprised of all the Russell–Saunders states associated with the $4f^3$ configuration. The values of the seven parameters (F_2, F_4, F_6, α, β, γ, and ζ_{so}) used in these calculations are listed in Table II.

The 4f-electron crystal field wave functions and energy levels were obtained by diagonalizing the appropriate crystal field Hamiltonians in a basis comprised of the 31 lowest energy intermediate-coupling states (multiplet levels). This basis was taken to be the same for all structures, and it included a total of 286 M_J levels. The parameters required in these calculations are the crystal field coefficients, $B_q^{(k)}$, of even parity (k = 2, 4, 6). These are defined by

$$H_{cf} = \sum_{k,q} B_q^{(k)} U_q^{(k)} \qquad (3)$$

where H_{cf} is the crystal field Hamiltonian and the $U_q^{(k)}$ are intraconfigurational unit tensor operators.[20] The $B_q^{(k)}$ coefficients are accessible to experimental determination *only* if one has spectra resolved at the crystal field level (i.e., spectra in which individual crystal field transitions can be resolved and assigned). This is not the case for our room-temperature solution-phase spectra, so we had to estimate the values of these coefficients from calculations based on the methods described in sections 2 and 3.4 of ref 8. These methods produce only rough estimates of the $B_q^{(k)}$ values, but they are based on a model of lanthanide–ligand interactions that is entirely consistent with our electric dipole intensity model for 4f → 4f transitions.[8] Quite accurate values of the $B_q^{(k)}$ coefficients would be required if our objective was to calculate distributions of electric dipole intensity among the crystal field components of multiplet-to-multiplet transitions (such as $^4I_{9/2} \rightarrow {}^4G_{5/2}$ and $^2G_{7/2}$). However, our more modest objective of calculating *overall* (or total) multiplet-to-multiplet transition strengths and intensities is much less demanding with regard to a detailed knowledge of the $B_q^{(k)}$ values.

The $B_q^{(k)}$ values used in all of the crystal field calculations reported here are listed in Table III. Note that $B_6^{(6)}$ is a complex number for the C_{3h} crystal fields of structures **4** and **5**.

(16) Rajnak, K.; Couture, L. *Chem. Phys.* **1981**, *55*, 331.
(17) Favas, M. C.; Kepert, D. L. *Prog. Inorg. Chem.* **1981**, *28*, 309.
(18) Foster, D. R.; Richardson, F. S. *Inorg. Chem.* **1983**, *22*, 3996.
(19) Salama, S.; Richardson, F. S. *J. Phys. Chem.* **1980**, *84*, 512.
(20) Hufner, S. "Optical Spectra of Transparent Rare Earth Compounds"; Academic Press: New York, 1978.

Table III. Even-Parity Crystal Field Coefficients Used in Energy Level Calculations[a]

	structures				
	1	2	3	4	5
$B_0^{(2)}/cm^{-1}$	722	−498	−637	−1632	−1561
$B_0^{(4)}/cm^{-1}$	−1191	−1964	−2219	550	589
$B_3^{(4)}/cm^{-1}$	*b*	−1008	−952	*b*	*b*
$B_0^{(6)}/cm^{-1}$	−135	356	264	854	858
$B_3^{(6)}/cm^{-1}$	*b*	313	323	*b*	*b*
$B_6^{(6)}/cm^{-1}$ [c]	538	275	126	339 (−1.52)	320 (7.73)

[a] Crystal field coefficients $B_q^{(k)}$ are defined according to eq 3. [b] These coefficients vanish by symmetry. [c] The $B_6^{(6)}$ coefficient has both real and imaginary parts in the C_{3h} symmetry of structures 4 and 5. The imaginary part is given in parentheses.

Table IV. Charge (q) and Polarizability ($\bar{\alpha}$) Parameters Assigned to the ODA, DPA, IDA, and MIDA Ligands

	ODA		DPA		IDA		MIDA	
site[a,b]	q/e	$\bar{\alpha}$/Å^3	q/e	$\bar{\alpha}$/Å^3	q/e	$\bar{\alpha}$/Å^3	q/e	$\bar{\alpha}$/Å^3
O(1)*	−0.20	0.65						
O(2)*	−1.15	0.91	−1.15	0.91	−1.15	0.91	−1.15	0.91
O(3)	−0.44	0.84	−0.44	0.84	−0.44	0.84	−0.44	0.84
C(1)	−0.04	1.03			0.09	1.03	0.09	1.03
C(2)	0.57	1.03	0.57	1.03	0.57	1.03	0.57	1.03
N(1)*			0	0	−0.15	1.19	−0.15	1.19
H(1)	0.08	0.41			0.08	0.41	0.08	0.41
H(N)					0.08	0.41		
Me(N)							0.33	2.26
py				9.66				

[a] Key: O(1), ether oxygen atom in ODA; O(2), coordinated oxygen atom of the carboxylate group; O(3), uncoordinated oxygen atom of the carboxylate group; C(1), methylene carbon atom; C(2), carboxylate carbon atom; N(1), nitrogen donor atom in DPA, IDA, and MIDA; H(1), methylene hydrogen atom; H(N), amine hydrogen in IDA; Me(N), methyl substituent in MIDA; py, centroid of the pyridyl moiety in DPA. [b] Asterisks denote ligating atoms.

Transition Dipole Strengths. Electric and magnetic dipole transition strengths were calculated by using precisely the same model and procedures described in ref 8. The radial parameters, $\langle r^\lambda \rangle$, and interconfigurational interaction parameters, $\Xi(t,\lambda)$, required for calculating the electric dipole strengths are given in Table II. The $\Xi(t,\lambda)$ values are those of Krupke.[21] The values of $\langle r^\lambda \rangle$ are the same as those used in our calculations of the $B_q^{(k)}$ coefficients. They are those given by Freeman and Watson.[22]

Three types of ligand parameters were required for our electric dipole strength calculations: (1) atomic (or perturber site) positional coordinates; (2) perturber site charges (q); (3) perturber site dipolar polarizabilities ($\bar{\alpha}$), assumed to be isotropic in this study. The charge and polarizability parameters assigned to the ODA, DPA, IDA, and MIDA ligands are listed in Table IV. Note that for DPA the polarizability of the pyridyl moiety is located at the centroid (of mass) of the pyridine ring. In our calculations on structure **1** each of the water molecules was treated as a *point* perturber site with a charge of −0.3 e and a polarizability of 1.49 Å^3.

The structure parameters for **1–5** were adapted from X-ray crystallographic data reported for similar systems.[11-13,23] Structure determinations have been reported for a number of $Ln(ODA)_3^{3-}$ and $Ln(DPA)_3^{3-}$ complexes,[11,12] so in these cases (structures **2** and **3**) only the Ln–O and Ln–N bond distances were modified to values appropriate for Ln = Nd. $Ln(IDA)_3^{3-}$ and $Ln(MIDA)_3^{3-}$ complexes have not yet been isolated in the solid state. However, a crystal structure determination has been reported for the compound $Nd(IDA)Cl\cdot 3H_2O$.[13] The coordination polyhedron about each Nd^{3+} ion in this structure includes one terdentate Nd(IDA) chelate system. The ligand structure parameters of this sytem were used in constructing our structures **4** and **5**. The Nd-ligating atom distances used in each of our structures **1–5** are given in Table V.

Table V. Nd-Ligating Atom Distances (Å) for Structures 1-5

	structures				
Nd-L bond[a]	1	2	3	4	5
Nd-O(H_2O)	2.54				
Nd-O(1)		2.49			
Nd-O(2)		2.41	2.41	2.47	2.47
Nd-N(1)			2.49	2.49	2.49

[a] See Table IV for numbering of ligand atoms.

Table VI. Electric Dipole Strengths Calculated for the $^4I_{9/2} \rightarrow {}^4G_{5/2}$ and $^4I_{9/2} \rightarrow {}^2G_{7/2}$ Transitions of Structures 1-5

		electric dipole strength/10^{-5} D^2 [a]			
transition	structure	$D^{(s)}$	$D^{(d)}$	$D^{(s,d)}$	D(total)
$^4I_{9/2} \rightarrow {}^4G_{5/2}$	1	2.97	114	−27.7	89.1
	2	143	105	128	375
	3	153	512	354	1019
	4	53.2	3209	421	3683
	5	49.0	2896	363	3308
$^4I_{9/2} \rightarrow {}^2G_{7/2}$	1	3.05	40.2	−15.3	28.1
	2	130	118	49.1	297
	3	138	415	165	719
	4	22.7	396	54.9	473
	5	21.2	363	50.5	434

[a] $D^{(s)}$ = static-coupling contribution; $D^{(d)}$ = dynamic-coupling contribution; $D^{(s,d)}$ = static/dynamic-coupling cross-term contribution; D(total) = $D^{(s)} + D^{(d)} + D^{(s,d)}$.

All of the calculated results reported here were obtained with use of the electronic and structural parameters listed in Tables II–V and described above. A few additional calculations involving some parameter variations were carried out, but no attempt was made to "optimize" our choice of parameter values to match experimental observation. The latter could not be justified given the approximation inherent to our model and the uncertainties regarding the actual structures of the complexes in solution.

There are three types of contributions to the electric dipole strengths calculated according to the model employed in the present study.[8,24] These are the static-coupling ($D^{(s)}$), dynamic-coupling ($D^{(d)}$), and static/dynamic-coupling cross-term ($D^{(s,d)}$) contributions. The mechanisms underlying each of these contributions have been discussed elsewhere.[8,24] The static-coupling contributions are related to the original Judd–Ofelt theory of 4f → 4f electric dipole intensities,[25,26] the dynamic-coupling contributions are related to the Mason–Peacock "ligand polarization" model,[1,7] and the cross-term contributions arise from interference effects between the static-coupling and dynamic-coupling transition moments.[24] Among the parameters introduced in our model, $D^{(s)}$ depends upon the $\Xi(t,\lambda)$ and ligand charge (q) parameters, $D^{(d)}$ depends on the $\langle r^\lambda \rangle$ and ligand polarizability ($\bar{\alpha}$) parameters, and $D^{(s,d)}$ has dependence on all four of these parameter sets. Each of the dipole strength contributions exhibits a different dependence on ligand geometry.

Calculated Results. Electric dipole strengths calculated for the $^4I_{9/2} \rightarrow {}^4G_{5/2}$ and $^2G_{7/2}$ transitions of structures **1–5** are given in Table VI, and electric dipole strengths calculated for the $^4I_{9/2} \rightarrow {}^2K_{13/2}$, $^4G_{7/2}$, and $^4G_{9/2}$ transitions are given in

(21) Krupke, W. F. *Phys. Rev.* **1966**, *145*, 325.
(22) Freeman, A. J.; Watson, R. E. *Phys. Rev.* **1962**, *127*, 2058.
(23) Helmholz, L. *J. Am. Chem. Soc.* **1939**, *61*, 1544.
(24) Richardson, F. S. *Chem. Phys. Lett.* **1982**, *86*, 47.
(25) Judd, B. R. *Phys. Rev.* **1962**, *127*, 750.
(26) Ofelt, G. S. *J. Chem. Phys.* **1962**, *37*, 511.

Table VII. Electric Dipole Strengths Calculated for the $^4I_{9/2} \rightarrow {}^2K_{13/2}$, $^4I_{9/2} \rightarrow {}^4G_{7/2}$, and $^4I_{9/2} \rightarrow {}^4G_{9/2}$ Transitions of Structures 1-5

transition	structure	electric dipole strength/10^{-5} D^2 [a] $D^{(s)}$	$D^{(d)}$	$D^{(s,d)}$	D(total)
$^4I_{9/2} \rightarrow {}^2K_{13/2}$	1	2.46	8.02	−2.89	7.60
	2	52.2	20.8	3.52	76.6
	3	49.7	44.5	13.0	107
	4	8.72	41.9	5.71	56.3
	5	9.06	39.5	5.00	53.5
$^4I_{9/2} \rightarrow {}^4G_{7/2}$	1	1.72	19.2	−6.27	14.6
	2	40.0	17.6	−2.23	55.4
	3	42.4	60.9	13.7	117
	4	19.0	187	14.7	220
	5	18.2	167	11.7	197
$^4I_{9/2} \rightarrow {}^4G_{9/2}$	1	2.35	11.7	−4.57	9.51
	2	53.2	9.74	−7.01	55.9
	3	55.0	22.4	0.28	77.6
	4	13.4	23.1	1.23	37.8
	5	12.9	21.0	0.84	34.7

[a] $D^{(s)}$ = static-coupling contribution; $D^{(d)}$ = dynamic-coupling contribution; $D^{(s,d)}$ = static/dynamic-coupling cross-term contribution; D(total) = $D^{(s)} + D^{(d)} + D^{(s,d)}$.

Table VIII. Comparison of Calculated vs. Experimentally Measured Oscillator Strengths

transitions	calcd[a] structure	$f/10^{-6}$	exptl[b] ligand	$f/10^{-6}$
$^4I_{9/2} \rightarrow {}^4G_{5/2}, {}^2G_{7/2}$	1	1.13	H_2O	8.65
	2	6.72	ODA	12.8
	3	16.9	DPA	19.2
	4	38.5	IDA	18.0
	5	36.6	MIDA	17.5
			MAL	16.1
			EHPG	19.6
$^4I_{9/2} \rightarrow {}^2K_{13/2}, {}^4G_{7/2}, {}^4G_{9/2}$	1	0.64	H_2O	6.20
	2	3.92	ODA	8.06
	3	5.96	DPA	11.2
	4	4.34	IDA	9.23
	5	3.98	MIDA	8.64
			MAL	8.21
			EHPG	10.3

[a] From eq 4, with use of the electric dipole strength results given in Tables VI and VII and $\chi = 1.19$. [b] From spectra obtained on solutions with $8 < pH < 10$.

Table VII. The latter transitions give an absorption band centered around 520 nm. The $|\Delta A|$ values observed within this absorption region are somewhat smaller than those observed within the $^4I_{9/2} \rightarrow {}^4G_{5/2}, {}^2G_{7/2}$ transition region (centered close to 580 nm), and the 520-nm absorption is not considered to be hypersensitive.

Comparisons of calculated vs. experimentally measured oscillator strengths are given in Table VIII for the $^4I_{9/2} \rightarrow {}^4G_{5/2}, {}^2G_{7/2}$ and $^4I_{9/2} \rightarrow {}^2K_{13/2}, {}^4G_{7/2}, {}^4G_{9/2}$ transitions of structures **1**–**5**. The calculated oscillator strengths were obtained from

$$f_{JJ'} = (8\pi^2 m_e c/he^2)\bar{\nu}_{JJ'}\chi(2J+1)^{-1}D_{JJ'} \qquad (4)$$

where $\bar{\nu}_{JJ'}$ is the barycenter energy of the $J \rightarrow J'$ transition (expressed in wavenumbers), χ is a correction factor for bulk refractivity effects (set equal to 1.19 for our aqueous solutions), and $D_{JJ'}$ is a multiplet (J)-to-multiplet (J') electric dipole strength. The $D_{JJ'}$ (total) values listed in Tables VI and VII were used in obtaining the calculated oscillator strengths given in Table VIII.

One of the most striking features of the calculated results shown in Table VIII is the order-of-magnitude underestimate of the oscillator strengths obtained for the $NdCl_3$(aq) system. Small parameter variations in our calculations on structure **1**, while maintaining exact D_{3h} point group symmetry, do not significantly improve our predicted f values (compared to experiment). However, small distortions of the structure away from D_{3h} symmetry can produce an order-of-magnitude increase in the calculated f values. It is possible that our idealized $Nd(H_2O)_9^{3+}$ structure (**1**) provides a relatively poor representation of the real species present in the $NdCl_3$(aq) system. On the other hand, it is also possible that the neglect of vibronic interactions in our electric dipole intensity model is responsible for our underestimates of the f values in the case of $NdCl_3$(aq). It is unlikely, however, that vibronic effects on the $4f \rightarrow 4f$ intensities of $Nd(H_2O)_9^{3+}$ would be greater than those for the other Nd/ligand systems examined in this study. We note that the oscillator strengths calculated for structures **2**–**5** are in every case within a factor of 2.1 of the experimentally determined values. This agreement is quite remarkable given the approximations inherent to our formal intensity model and our structural models for the respective complexes.

Table IX. Relative Oscillator Strengths

transitions	calcd[a] structure	f(relative)*	f(relative)**	exptl[b] ligand	f(relative)
$^4I_{9/2} \rightarrow {}^4G_{5/2}, {}^2G_{7/2}$	1	0.17	0.08	H_2O	0.67
	2	1.00	1.00	ODA	1.00
	3	2.51	1.88	DPA	1.50
	4	5.71	2.42	IDA	1.41
	5	5.45	2.33	MIDA	1.37
$^4I_{9/2} \rightarrow {}^2K_{13/2}, {}^4G_{7/2}, {}^4G_{9/2}$	1	0.16	0.10	H_2O	0.79
	2	1.00	1.00	ODA	1.00
	3	1.52	1.35	DPA	1.39
	4	1.11	1.02	IDA	1.15
	5	1.02	0.91	MIDA	1.08

[a] Each transition set is considered separately, with f(relative) for structure 2 being arbitrarily set equal to 1.00 in each case. The f(relative)* values were calculated by using the dipole strength results given in Tables VI and VII. The f(relative)** values were calculated by using dipole strengths in which the dynamic-coupling contributions to the electric dipole transition moments were each multiplied by a scaling factor of 0.5. [b] From the data given in Table VIII, with f(ODA) = 1.00 for each transition set.

We note from Tables VI and VII that the static-coupling mechanism contributes significantly to the dipole strengths of structure **1** *only* through the $D^{(s,d)}$ cross terms. For this structure, these terms are calculated to make *subtractive* contributions to D(total). Recall that negative values for the $D^{(s,d)}$ terms arise from destructive interferences between the static- and dynamic-coupling electric dipole transition vectors.[24]

Considering the $^4I_{9/2} \rightarrow {}^4G_{5/2}, {}^2G_{7/2}$ dipole strength results given in Table VI for structures **2**–**5**, we note the following $D^{(d)}$:$D^{(s)}$ ratios: 0.82 (**2**), 3.19 (**3**), 47.5 (**4**), 46.5 (**5**). For structures **4** and **5**, the dynamic-coupling mechanism *alone* is predicted to contribute ~87% of the total electric dipole strength, while for structures **2** and **3** it is predicted to contribute ~33% and ~53%, respectively. The static-coupling mechanism is predicted to make the dominant contribution only for structure **2** (~41% of D(total)). From Table VIII, we see that the oscillator strengths calculated for structures **4** and **5** are about twice as large as those experimentally determined for the corresponding Nd/ligand complexes, while those calculated for structures **2** and **3** are underestimated by factors of 1.9 and 1.1, respectively.

In Table IX, we list *relative* oscillator strengths calculated and observed within each transition region, $^4I_{9/2} \rightarrow {}^4G_{5/2}, {}^2G_{7/2}$ and $^4I_{9/2} \rightarrow {}^2K_{13/2}, {}^4G_{7/2}, {}^4G_{9/2}$, setting f(relative) = 1.00 for structure **2** and for $Nd(ODA)_3^{3+}$. The f(relative)* values were calculated using the dipole strength results given in Tables VI and VII. The f(relative)** values were calculated using dipole strengths in which the dynamic-coupling contributions to the

electric dipole transition moments were each scaled by a factor of 0.5. The latter scales the $D^{(s,d)}$ contributions by a factor of 0.5 and the $D^{(d)}$ contributions by a factor of 0.25. This scaling of the dynamic-coupling contributions brings the calculated oscillator strengths for structures **4** and **5** into closer agreement with experiment in the $^4I_{9/2} \rightarrow {}^4G_{5/2}, {}^2G_{7/2}$ transition region. Nearly all of the dynamic-coupling contributions to the $^4I_{9/2} \rightarrow {}^4G_{5/2}, {}^2G_{7/2}$ *and* $^4I_{9/2} \rightarrow {}^2K_{13/2}, {}^4G_{7/2}, {}^4G_{9/2}$ electric dipole transition moments arise from the quadrupole (Nd)-induced dipole (ligand) interaction terms in the dynamic-coupling intensity model. Each of these terms has a $\langle r^2 \rangle$ dependence, so our 0.5 scaling factor can be thought of as a "shielding" correction applied to the Freeman and Watson[22] $\langle r^2 \rangle$ radial expectation value for the 4f electrons. The possible importance of applying such a correction to the Freeman and Watson $\langle r^\lambda \rangle$ values when calculating ligand field dependent properties has been discussed elsewhere (see ref 20, page 72).

The *relative* values of $D^{(d)}:D^{(s)}$ calculated for the $^4I_{9/2} \rightarrow {}^4G_{5/2}, {}^2G_{7/2}$ transitions of structures **2** and **3** vs. those of structures **4** and **5** reflect, primarily, geometrical (and symmetry) effects. Assuming *isotropic* ligand polarizabilities, certain dynamic-coupling contributions to electric dipole strength can be shown to be allowed in C_{3h} symmetry (as in structures **4** and **5**) but forbidden in D_3 symmetry (as in structures **2** and **3**).[27] This, in large part, accounts for the larger $D^{(d)}$ values calculated for structures **4** and **5** vs. those calculated for structures **2** and **3**. The larger $D^{(s)}$ values calculated for **2** and **3** vs. those calculated for **4** and **5** can also be traced to geometry-dependent effects. Reid and Richardson[27,28] have shown that inclusion of ligand polarizability *anisotropy* in the dynamic-coupling intensity mechanism can lead to additional contributions to $D^{(d)}$ (and to $D^{(s,d)}$). For the $^4I_{9/2} \rightarrow {}^4G_{5/2}, {}^2G_{7/2}$ transitions of structures **2**–**5**, these additonal contributions would be expected to be greatest for **2** and **3** (i.e., those having D_3 symmetry). In all the calculations reported here, only *isotropic* ligand polarizabilities were considered.

Discussion

The data given in Table I and the difference spectra shown in Figures 1–9 clearly demonstrate the hypersensitive behavior of the $^4I_{9/2} \rightarrow {}^4G_{5/2}, {}^2G_{7/2}$ absorption band. At pH values >6.5, the ligands producing the *largest* increases in oscillator strength (over that for $NdCl_3(aq)$) are EHPG and DPA, followed by IDA and MIDA. Both EHPG and DPA have highly polarizable aromatic donor moieties (the phenolate groups in EHPG and the pyridyl group in DPA), which serve to distinguish them from the other ligands included in this study. The ligands producing the *smallest* increases in oscillator strength at pH values >6.5, ODA and MAL, are distinguished from the other ligands by their lack of any nitrogen donor atoms. The EHPG ligand contains two amino groups, IDA and MIDA each contain one amino group that can bind, and DPA has the pyridyl nitrogen donor atom.

With respect to coordination number and symmetry, the 1:3 Nd^{3+}:ODA and Nd^{3+}:DPA systems are most likely isostructural in solution at pH >6.5 (the dominant species being tris terdentate complexes with D_3 symmetry).[18] The rather significant differences in their respective spectra (see Figures 1, 2, and 6) and Δf values (see Table I), therefore, must be attributable to differences between how the $-CH_2OCH_2-$ and pyridyl moieties interact with the 4f electrons of the Nd^{3+} ion. The 1:3 Nd^{3+}:IDA and Nd^{3+}:MIDA systems are also expected to be isostructural (with respect to coordination number and symmetry) in solution at pH >6.5. In these cases, the dominant species are most likely tris terdentate complexes having C_{3h} symmetry.[18,19] The Δf and f values measured for these systems are quite similar (see Tables I and VIII), indicating that the NH (in IDA) and NCH_3 (in MIDA) groups contribute similarly to f → f intensity. Note, however, that the spectra shown in Figure 9 suggest differences in the crystal field splittings produced by the IDA and MIDA ligands.

The spectra obtained for the 1:3 Nd^{3+}:ODA and Nd^{3+}:DPA systems exhibit very little change (qualitatively and quantitatively) over the range pH 3–9 (see Figures 1 and 2). The spectra obtained for the 1:3 Nd^{3+}:IDA and Nd^{3+}:MIDA systems, on the other hand, exhibit very significant qualitative and quantitative changes over the interval pH 4–6. This can be explained in the following way: whereas the middle (weak) donor atoms in the ODA and DPA ligands are *forced* into coordination sites upon binding by the terminal carboxylate groups (at pH ≲3), the middle donor atoms (nitrogens) of the IDA and MIDA ligands are *not* forced into coordination sites upon carboxylate binding. (Recall that the bicyclic chelate systems formed by ODA and DPA upon binding must be nearly planar, while for IDA and MIDA they cannot be planar.) The nitrogen atoms of the IDA and MIDA ligands are not coordinated at pH <4, and terdentate chelation by these ligands is not complete until pH >6. For ODA and DPA, on the other hand, terdentate chelation can occur in the carboxylate binding region (pH <3).

The $^4I_{9/2} \rightarrow {}^4G_{5/2}, {}^2G_{7/2}$ spectrum of the 1:1 Nd^{3+}:EHPG system also exhibits a dramatic increase in intensity on going from low pH to high pH (see Table I and Figure 5). This increase is greatest in the pH 5–7 region. Over this range (pH 5–7), the two phenolic groups of the ligand are being deprotonated and are entering the inner coordination sphere.[14] It has been proposed in the case of 1:1 Tb^{3+}:EHPG that by pH 7 the ligand is fully hexacoordinated to the lanthanide ion via two carboxylate groups, two amino groups, and two phenolate groups.[14] It is reasonable to assume that 1:1 Nd^{3+}:EHPG would exhibit similar coordination properties. Hexacoordination (involving five chelate rings) and the presence of four negatively charged donor groups and two highly polarizable ligand moieties (the phenolate groups) give Nd^{3+}:EHPG many of the structural features thought to be important to 4f → 4f electric dipole intensity enhancement. Since the large increases in f(complex):f(aquo) occur over the pH region in which the phenolate groups are entering the coordination sphere, it is tempting to associate these increases with ligand polarization effects such as those envisioned by Mason and Peacock in their theory of hypersensitivity.[1,7] However, some caution must be exercised in this regard since it is certain that the geometry and "effective" symmetry of the ligand field about the lanthanide ion are also changing over this pH region, with respect to *both* the ligand charge and polarizability distributions. It may be that the observed intensity changes are due more to changes in ligand field geometry than to changes in ligand polarizability.

The pH dependence observed in the ΔA spectra of the 1:3 Nd^{3+}:malate system between pH 2 and pH 7 (see Figure 4) reflects the formation of tris bidentate $Nd(MAL)_3^{3-}$ complexes (completed by pH ~5) and the deprotonation of two coordinated water molecules (to OH^- ligands, between pH 5 and pH 7).[15] The rather dramatic changes in the shape and structure of the ΔA spectra observed upon raising the solution pH above 7 suggest that major alterations are occurring in the ligand environment. In our previous studies of 1:3 Tb^{3+}:MAL and 1:3 Eu^{3+}:MAL systems in aqueous solution,[15,29] we observed similarly dramatic changes in the luminescence and emission optical activity spectra when the pH

(27) Reid, M. F.; Richardson, F. S. *J. Chem. Phys.* **1983**, *79*, 5735.
(28) Reid, M. F.; Richardson, F. S. *Chem. Phys. Lett.* **1983**, *95*, 501.
(29) Brittain, H. G.; Richardson, F. S. *Inorg. Chem.* **1976**, *15*, 1507.

was raised above 7. In those cases, the large changes were attributed to the onset of *terdentate* chelation by at least one or two of the bound malate ligands (via two carboxylate groups *plus* the α-OH, *or* hydroxylate, group). The change from bidentate to terdentate chelation by the malate ligands would be expected to significantly alter the ligand field sensed by the Ln^{3+} 4f electrons and, thereby, induce major changes in the 4f → 4f optical spectra (especially in transition regions known to exhibit hypersensitive behavior).

Conclusions

The experimental results reported here clearly demonstrate the hypersensitive behavior of the $^4I_{9/2} \rightarrow {}^4G_{5/2}, {}^2G_{7/2}$ transitions of Nd(III), and it is shown how the absorption spectra associated with these transitions can be used to elicit information about complex formation (as a function of solution pH). Furthermore, it was shown how the *relative* $^4I_{9/2} \rightarrow {}^4G_{5/2}, {}^2G_{7/2}$ absorption intensities observed for the various systems could be rationalized (at least qualitatively) in terms of specific ligand structural features such as (1) the nature and number of donor groups, (2) the nature and number of nonligating substituent groups, and (3) chelate-ring conformational properties. Our direct calculations of transition oscillator strengths (for model structures presumed to be similar to the real structures present in solution at pH >7) met with mixed success. Agreement between the calculated vs. experimentally determined oscillator strengths was good (in some cases, excellent) for the tris terdentate chelate structures **2-5**. However, our calculations grossly underestimated the oscillator strengths for the $NdCl_3$(aq) system (modeled as a 9-coordinate $Nd(H_2O)_9^{3+}$ complex with exact D_{3h} symmetry). This led to significant overestimates of f(complex):$f(NdCl_3(aq))$ ratios and hypersensitive behavior. It is likely that this problem can be attributed primarily to the inappropriateness of using our idealized structure **1** to model the complexes present in the $NdCl_3$(aq) system.

Acknowledgment. This work was supported by the National Science Foundation (NSF Grant CHE-8215815).

Registry No. $Nd(ODA)_3^{3-}$, 43030-80-4; $Nd(DPA)_3^{3-}$, 38721-35-6; $Nd(IDA)_3^{3-}$, 12561-55-6; $Nd(MIDA)_3^{3-}$, 89746-87-2; $Nd(MAL)_3^{3-}$, 89773-17-1; NdEHPG$^-$, 89746-88-3.

Contribution from the Department of Chemistry,
The Pennsylvania State University, University Park, Pennsylvania 16802

Europium(III) Luminescence Excitation Spectroscopy. A Species-Specific Method for the Quantitation of Lanthanide Ion Binding to Chelating Agents. Complexes of (1,2-Ethanediyldioxy)diacetate

MICHAEL ALBIN, GREGORY K. FARBER, and WILLIAM DEW. HORROCKS, JR.*

Received September 1, 1983

Laser excitation spectroscopy was used to monitor the complexation of (1,2-ethanediyldioxy)diacetate (EDA^{2-}) with lanthanide(III) ions. Relative formation constants for the 1:1 species were determined in competition experiments that monitor the decrease in the excitation maximum due to $Eu(EDA)^+$ as $Ln(EDA)^+$ is formed. The formation constant, K_2, for the bis complex, $Eu(EDA)_2^-$, was evaluated by following the changes in the $^7F_0 \rightarrow {}^5D_0$ excitation spectrum as a function of the concentration of added EDA^{2-}. Excited-state lifetime measurements in H_2O and D_2O solution provided the number of coordinated water molecules in the two complexes (7 and 3 for the mono and bis complexes, respectively). Structural comparisons between solid-state and solution species were made from the excitation spectra.

Introduction

Classical methods for the determination of the binding constants of metal ions to chelating ligands generally involve fitting the results of potentiometric titrations of the ligand in the presence and absence of metal ion to a sometimes complex scheme requiring the knowledge of multiple proton dissociation constants.[1] These methods are necessarily indirect, and their validity depends upon the correctness of assumptions made concerning the species present in solution. Work in this laboratory has involved the exploitation of laser-excited europium(III) luminescence to monitor the binding of this ion to specific sites in proteins or individual complexes in solution. Our experiment involves excitation of the $^7F_0 \rightarrow {}^5D_0$ transition of Eu(III) by scanning a pulsed dye laser through the transition region (577-581 nm) while emission corresponding to the relatively intense $^5D_0 \rightarrow {}^7F_2$ transition (~614 nm) is monitored. Since the absorptive transition is between nondegenerate levels, the observation of more than one peak in the excitation spectrum implies the presence of more than one Eu(III) environment. These methods have been employed in this laboratory to quantitate Eu(III) ion binding to proteins,[2-8] ionophoric ligands,[9] and monodentate anions[10] as well as to monitor ligand-exchange kinetic processes in chelate systems.[11] In addition, from measurements of excited-state lifetimes made separately in H_2O and D_2O solution, it is possible to determine the number of water molecules coordinated to the Eu(III) ion in any given species.[2,12]

The present research illustrates the application of these species-specific methods to obtain two additional classes of

(1) Rossotti, F. J. C.; Rossotti, H. "The Determination of Stability Constants"; McGraw-Hill: New York, 1961.

(2) Horrocks, W. DeW., Jr.; Sudnick, D. R. *Acc. Chem. Res.*, **1981**, *14*, 384-392.
(3) Horrocks, W. DeW., Jr.; Sudnick, D. R. *Science (Washington, D.C.)* **1979**, *206*, 1194-1196.
(4) Rhee, M.-J.; Sudnick, D. R.; Arkle, V. K.; Horrocks, W. DeW., Jr. *Biochemistry* **1981**, *20*, 3328-3334.
(5) Snyder, A. P.; Sudnick, D. R.; Arkle, V. K.; Horrocks, W. DeW., Jr. *Biochemistry* **1981**, *20*, 3334-3339.
(6) Wang, C.-L.; Leavis, P. C.; Horrocks, W. DeW., Jr.; Gergely, J. *Biochemistry* **1981**, *20*, 2439-2444.
(7) Rhee, M.-J.; Horrocks, W. DeW., Jr.; Kosow, D. P. *Biochemistry* **1982**, *21*, 4524-4528.
(8) Horrocks, W. DeW., Jr.; Mulqueen, P.; Rhee, M.-J.; Breen, P. J.; Hild, E. K. *Inorg. Chim. Acta* **1983**, *79*, 24-25.
(9) Albin, M.; Goldstone, A. C.; Withers, A. S.; Horrocks, W. DeW., Jr. *Inorg. Chem.* **1983**, *22*, 3182-3184.
(10) Breen, P. J.; Horrocks, W. DeW., Jr. *Inorg. Chem.* **1983**, *22*, 536-540.
(11) Horrocks, W. DeW., Jr.; Arkle, V. K.; Liotta, F. J.; Sudnick, D. R. *J. Am. Chem. Soc.* **1983**, *105*, 3455-3459.
(12) Horrocks, W. DeW., Jr.; Sudnick, D. R. *J. Am. Chem. Soc.* **1979**, *101*, 334-340.

0020-1669/84/1323-1648$01.50/0